Shenlian Extract in the Treatment of Ultrafine Particulate Matter- Aggravated Myocardial Ischemic Injury: Integrating Network Pharmacology and in vivo Pharmacological Evaluation

Shuiqing Qu

Artemisinin Research Center, China Academy of Chinese Medical Sciences, Beijing China. 2 Institute of Chinese Materia Medica, China Academy of Chinese Medical Sciences, Beijing China. 3 School of Tranditional Chinese Medicine，GDPU.

Kai Li

Artemisinin Research Center, China Academy of Chinese Medical Sciences, Beijing China. 2 Institute of Chinese Materia Medica, China Academy of Chinese Medical Sciences, Beijing China. 3 School of Tranditional Chinese Medicine，GDPU.

Ting Yang

Artemisinin Research Center, China Academy of Chinese Medical Sciences, Beijing China. 2 Institute of Chinese Materia Medica, China Academy of Chinese Medical Sciences, Beijing China. 3 School of Tranditional Chinese Medicine，GDPU.

Yuanmin Yang

Artemisinin Research Center, China Academy of Chinese Medical Sciences, Beijing China. 2 Institute of Chinese Materia Medica, China Academy of Chinese Medical Sciences, Beijing China.

Zhongyuzn Zheng

Artemisinin Research Center, China Academy of Chinese Medical Sciences, Beijing China. 2 Institute of Chinese Materia Medica, China Academy of Chinese Medical Sciences, Beijing China.

Hui Liu

Artemisinin Research Center, China Academy of Chinese Medical Sciences, Beijing China. 2 Institute of Chinese Materia Medica, China Academy of Chinese Medical Sciences, Beijing China. 3 School of Tranditional Chinese Medicine，GDPU.

Xi Wang

Artemisinin Research Center, China Academy of Chinese Medical Sciences, Beijing China. 2 Institute of Chinese Materia Medica, China Academy of Chinese Medical Sciences, Beijing China.

Yu Zhang

Artemisinin Research Center, China Academy of Chinese Medical Sciences, Beijing China. 2 Institute of Chinese Materia Medica, China Academy of Chinese Medical Sciences, Beijing China.

Shuoqiu Deng

Artemisinin Research Center, China Academy of Chinese Medical Sciences, Beijing China. 2 Institute of Chinese Materia Medica, China Academy of Chinese Medical Sciences, Beijing China.

Xiaoxin Zhu

Institute of Chinese Materia Medica, China Academy of Chinese Medical Sciences, Beijing China.

Lina Chen

Artemisinin Research Center, China Academy of Chinese Medical Sciences, Beijing China. 2 Institute of Chinese Materia Medica, China Academy of Chinese Medical Sciences, Beijing China.

Yujie Li (yjli@icmm.ac.cn)

Artemisinin Research Center, China Academy of Chinese Medical Sciences, Beijing China. 2 Institute of Chinese Materia Medica, China Academy of Chinese Medical Sciences, Beijing China.

Research

Keywords: SL extract, Myocardial ischemic injury, Ultrafine Particle, Mechanism of action, Network 38 pharmacology, NOD-like signaling pathway

Posted Date: September 8th, 2020

DOI: https://doi.org/10.21203/rs.3.rs-62327/v1

Type of the Paper: Article

Shenlian Extract in the Treatment of Ultrafine Particulate Matter- aggravated Myocardial Ischemic Injury: Integrating Network Pharmacology and in vivo Pharmacological Evaluation

Shuiqing Qu[1,2,3#], Kai Li[1,2#], Ting Yang[1,2], Yuanmin Yang[1,2], Zhongyuzn Zheng[1,2], Hui Liu[1,2,3], Xi Wang[1,2],Yu Zhang[1,2] , Shuoqiu Deng[1,2], Xiaoxin Zhu[1*], Lina Chen[1,2*], Yujie Li [1,2*]

Abstract

Background: Air pollution is a growing public health burden associated with several negative health effects, especially cardiovascular disease. Shenlian extract (SL), a traditional Chinese medicine, has the effects of clearing heat-toxin and promoting blood circulation for removing blood stasis, and it has long been used to treat cardiovascular diseases and atherosclerosis. This study explored the underlying action mechanism of SL against ultrafine particle-induced myocardial ischemic injury (UFP-MI) through network pharmacology prediction and experimental verification.

Methods: Male Sprague-Dawley rats with UFP-MI were pre-treated with SL intragastrically for 7 days, all the animals were randomly divided into five groups: Sham, Model (UFP+MI), SLL(31.08mg/ kg·d) + UFP+ MI, SLM (62.16 mg/ kg·d) + UFP+MI, and SLH (124.32 mg/ kg·d) + UFP+ MI. SL or saline was administrated 7 days before UFP instillation (100 μg/kg), followed by 24 h of ischemia. Inflammatory cytokine detection and histopathological analysis were performed to assess the protective effects of SL. For the mechanism study, differentially expressed genes were identified in UFP-MI rats treated with SL through transcriptomic analysis. Subsequently, in combination with network pharmacology, potential pathways involved in the effects of SL treatment were identified using the Internet-based Computation Platform (www.tcmip.cn) and Cytoscape 3.6.0. Further validation experiments were performed to reveal the mechanism of the therapeutic effects of SL on UFP-MI.

Results: In pharmacodynamics experiments, SL significantly suppressed inflammatory cell infiltration into myocardial tissue and exhibited significant anti-inflammatory activity. Transcriptomic analysis revealed that the differentially expressed genes after SL treatment had significant anti-inflammatory, immunomodulatory, and anti-viral activities. Network pharmacology analysis illustrated that the targets of SL participate in the inflammatory response, apoptotic process, innate immune response, platelet activation, and other processes. By combining transcriptomic and network pharmacology data, we found that SL may exert anti-inflammatory effects by acting on the NOD-like signaling pathway to regulate immune response activation and inhibit systemic inflammation. Verification experiments revealed that SL suppressed NLRP3 inflammasome active and inflammasomes are cytosolic protein complexes that stimulate the activation of Caspase-1, which in turn induces the secretion of the inflammatory cytokines Interleukin-1 (IL-1), Interleukin-18(IL-18) and Interleukin-33(IL-33)

Conclusion: UFP can induce the activation of NLRP3 inflammasome, leading to the release of downstream the inflammatory cytokines, aggravate the pathological conditions of inflammatory infiltration, and further aggravate the myocardial ischemic injury. Experimental verification indicated that SL can directly inhibit the activation of NLRP3 inflammasomes in the NOD-like signaling pathway and reduce cytokines

release. In conclusion, our results confirmed that SL may prevent UFP-MI by acting on the NOD-like signaling pathway.

Keywords: SL extract; Myocardial ischemic injury; Ultrafine Particle; Mechanism of action; Network pharmacology; NOD-like signaling pathway

Authors' information

* Correspondence: Yujie Li, yjli@icmm.ac.cn; Lina Chen, lnchen@icmm.ac.cn; Xiaoxin Zhu, xxzhu@icmm.ac.cn

# These two authors contributed equally to this work

content

1 Background

Air pollution consists of a complex mixture of gases and particulate matter, and it is recognized as a major contributor to morbidity and mortality worldwide, particularly cardiovascular mortality [1-3]. According to the World Health Organization, air pollution causes an estimated 4.2 million deaths annually, and 91% of the world's population resides in regions in which the air quality does not meet World Health Organization recommendations [4]. In epidemiologic studies, hypertension, type 2 diabetes, overweight or obesity, hypertriglyceridemia, and hyperbetalipoproteinemia increased the susceptibility to the cardiovascular effects of air pollution [5].

To a certain extent, fine particulate matter, also known as ultrafine particles (UFPs), comprises all particles with a diameter of less than 1 μm. UFPs in air pollutants are primary pathogenic factors because of their high numbers, and they possess a large surface area, allowing a substantial amount of toxic chemicals to be adsorbed [6, 7]. UFPs can pass through the respiratory tract to the alveoli with high efficiency. A small fraction of UFPs penetrates the alveolar–capillary barrier, permitting their distribution throughout the body via the circulatory system [8,9]. It is not completely clear when exposure to air pollution, especially UFPs, results in damage to the cardiopulmonary system.

There are various plausible hypothesized pathophysiological mechanisms linking exposure to air pollutants to cardiovascular disease (CVD), including systemic inflammation and oxidative stress, autonomic nervous system imbalance, and abnormal epigenetic changes. Susceptible populations with cardiometabolic risk factors might be more susceptible to the pro-inflammatory effects of air pollutants, leading to a higher prevalence of CVD [10]. Prior research indicated that long-term exposure to particulate matter can result in newly formed plaques, which can develop into fibrous fatty plaques that are prone to breakage and instability [10]. This mechanism has also been demonstrated in animal models, in which exposure to higher levels of particulate matter potentiated atherosclerosis by increasing the generation of reactive oxygen species, inducing vascular inflammation, and promoting lipid metabolism disorder and the instability of plaques [11,12]. In addition, epidemiological research illustrated that the severity of coronary artery disease on invasive coronary angiography increases with higher long-term exposure to particulate matter [13].

Shenlian extract (SL), a traditional Chinese medicine (TCM), carries the effects of clearing heat-toxin and promoting blood circulation for removing blood stasis, and it has long been used to treat CVD and atherosclerosis. Previous studies found that SL can effectively inhibit the formation of atherosclerotic plaques [14], maintain the stability of plaques[15], ameliorate local blood flow, and improve blood lipid levels[14]. Additionally, some studies demonstrated that SL can affect the transformation of macrophage phenotype and the secretion of M1 macrophage inflammatory factors and regulate the nuclear factor (NF)-κB signaling pathway to inhibit the inflammation of macrophages[16,17]. Recent research based on a model of myocardial ischemic injury (MI) in anesthetized dogs, ex vivo rat hearts, and H9c2 cardiomyocytes illustrated that SL can reduce the severity of myocardial ischemia and the scope of myocardial ischemia. Meanwhile, SL can protect against myocardial ischemic injury through the NF-κB signaling pathway [18].

Network pharmacology, which is based on big databases, examines signaling from the molecular level to the pathway level, and it has emerged as a useful tool for the detailed description of the action mechanisms of complicated drug systems [19]. The previous mode of "one target, one drug" has been updated to a new mode termed "network target, multi-components" [20, 21] Network pharmacology can be used to evaluate the rationality and compatibility of TCM by clarifying detailed compound-target and target-pathway networks. In the current study, we combined network pharmacology prediction and

experimental verification to explore the underlying action mechanism of SL in a rat model of UFP-aggravated MI (UFP-MI).

2 Materials and Methods

2.1 Chemicals and reagents

SL [22](Li Yu-jie, et al.,2011; Guo, et al.,2016) is a modern TCM formula. It is made from the extracts of two Chinese medicines, namely Salvia miltiorrhiza Bunge and Andrographis paniculata (Burm. f.)Nees. SL was prepared via alcohol extraction and macroporous resin enrichment and purification. SL contained 3% tanshinone II A, 38% salvianolic acid B, and 20% andrographolide, which were provided by the Chemical Laboratory of Institute of Chinese Materia Medica, Chinese Academy of Sciences (Beijing, China). Briefly, Salvia miltiorrhiza Bunge and Andrographis paniculata（Burm. f.）Nees were mixed at the ratio of 15:9, that were first extracted using ethanol followed by water.

All chemicals used in the study were purchased from Sigma-Aldrich (St. Louis, MO, USA) unless specifically indicated. Diesel particulate matter was purchased from the National Institute of Standards and Technology of the United States. Its main chemical components are polycyclic aromatic hydrocarbons (PAHs) and nitro-polycyclic aromatic hydrocarbons (Nitro-PAHs), and its average particle size is approximately 0.18 um.

2.2 Animals and treatments

This study was performed according to the instructions of the Guide for the Care and Use of Laboratory Animals and the guidelines of Institute of Chinese Materia Medica Animal Research Committee. Male 8-week-old SPF Sprague-Dawley rats (200 ± 20 g) were obtained from Beijing HFK Biotechnology Co., LTD. The rats were acclimated for 2–3 days under controlled temperature (24 ± 2°C), relative humidity of 60 ± 5%, and a 12-h/12-h light/dark cycle, and animals were provided a normal diet and water daily for the duration of the experiments. Male Sprague-Dawley rats with UFP-MI were pre-treated with SL intragastrically for 7 days, all the animals were randomly divided into five groups: Sham, Model (UFP+MI), SLL(31.08 mg/ kg. d) + UFP+ MI, SLM (62.16 mg/ kg. d) + UFP+MI, and SLH (124.32 mg/ kg. d) + UFP+ MI. SL or saline was administrated 7 days before UFP instillation (100 μg/kg), followed by 24 h of ischemia.

2.3 Preparation of the UFP suspension

An appropriate amount of SRM1650b powder was precisely weighed using a 1/100 000 electronic analytical balance and placed in an Eppendorf tube. The final concentration of the suspension was 1 mg/mL, which was generated by adding the corresponding volume of phosphate buffer solution. After mixing, the particles were evenly distributed via ultrasound for 2 h, and the mixture frozen at −20°C for storage.

2.4 Intratracheal instillation method of the UFP suspension

The preparations were sonicated for 30 min and vortexed immediately (<60 s) prior to intratracheal instillation. Rats were anesthetized via an intraperitoneal injection. A volume of the UFP suspension (1 mL/kg) was instilled intratracheally via a plastic, blunt cannula (1.20 mm gauge diameter). The same amount of PBS was instilled into the lungs of control rats.

2.5 Establishment of a rat model of myocardial ischemia

MII was induced by surgical ligation of the left anterior descending coronary artery (LAD) [23] (Zhang, et al., 2019). Healthy male Sprague-Dawley rats (weight, 180–220 g) were used for the studies. After anesthesia and successful endotracheal intubation, the rats were connected to a ventilator, and their chests

were opened at the left between the third and fourth intercostal spaces to expose the heart. The LAD was ligated using a 5-0 silk suture that was inserted 2–3 mm below the junction between the left atrial appendage and conus arteriosus and removed 1–2 mm below the lower margin of the left atrial appendage. Successful ligation was verified by a color change.

2.6 RNA extracting and sequencing

RNA preparation, library construction, and sequencing were performed by CapitalBio Technology Co., LTD (Beijing, China) using their high-throughput genome sequencing platform. Briefly, flash-frozen heart tissues samples were homogenized in TRIzol® reagent, and total RNA was generated according to the manufacturer's protocol. The new-generation Illumina high-throughput sequencing platform was used to perform sequence splicing and assembly to obtain single gene clusters. According to different sequencing types and sequencing lengths, we selected the correct recipe and constructed the mRNA library. Compared with bioinformatics-related databases, when a gene was upregulated in the model group and downregulated in the SL group or vice versa, it was regarded as differentially expressed.

2.7 Prediction of the candidate targets of SL

The TCMIP database contains the ingredients of herbs and formulas from ETCM (http://www.ehbio.com/ETCM) that were collected manually according to the Pharmacopoeia of the People's Republic of China (2015 version) and other literature[24] (Xu, et al., 2019). In this study, the corresponding targets of SL were obtained from the TCMIP V2.0 database using Salvia miltiorrhiza Bunge and Andrographis paniculata（Burm. f.）Nees as keywords[25,26] (Cui Ru-yi, Xu Hai-yu, 2019; Zhang Qian-tao,et al.,2019). In the target prediction function module of TCM, the two-dimensional structural similarity of chemical components was compared with the drugs listed by The US Food and Drug Administration, and the similarity score was obtained by the similarity measurement method defined by the Tanimoto score[27](Xu, et al.,2019). Accordingly, the therapeutic targets in the DrugBank database of known drugs are considered the candidate targets of the herbal ingredients with Tanimoto scores ≥ 0.8 for the known drugs. We choose drug targets with similarity scores ≥ 0.8 as the candidate targets of SL.

2.8 Prediction of particulate matter and CVD targets

Known targets related to CVD were screened using diseases and disease phenotypes as keywords from the Therapeutic Target Database (TTD, http://systemsd-ock.unit.osit.jp/iddp/home/index), the DisGeNET Database (https://www.disgenet.org/), the DrugBank database (https://www.drugbank.ca), Human Phenotype Ontology (https://hpo.jax.org/app/), and research articles. At the same time, the pathological toxicological processes caused by particulate matter were searched in research articles to identify relevant pathogenic targets.

2.9 The candidate SL target network construction and enrichment analysis

A target interaction (protein–protein interaction [PPI]) network was built by importing the gene names into the public database STRING. The relation schema of targets was drawn using Cytoscape software. Cytoscape 3.6.0 was used as a tool to visualize the PPI network. Furthermore, it supplies a basic set of features for data integration, analysis, and visualization for complicated network analysis.

2.10 Construction of the interaction network of transcriptome differential genes and network targets

Using the PPI module to construct the map of the core target network through transcriptome differential genes and network targets, the platform was set to the key core targets with values exceeding the node's median for "Degree," "Betweenness," and "Closeness" as the therapeutic targets of SL for the treatment of UFP-MI.

2.11 Enrichment analysis

Gene Ontology and Kyoto Encyclopedia of Genes and Genomes pathway enrichment analyses were also performed on the target data using the Database for Annotation, Visualization, and Integrated Discovery[28] (Xie, et al.,2018). Gene Ontology enrichment analysis of biological process, molecular function, cellular component, and Kyoto Encyclopedia of Genes and Genomes pathways was performed [21] (Guo, et al., 2019). The main signaling pathways of the core targets were obtained to investigate the possible mechanism of action of SL in the treatment of UFP-MII.

2.12 Experimental validation

2.12.1 Western blotting

After obtaining myocardial tissue and extracting the total protein, bovine serum albumin (Sigma-Aldrich) was used as a standard to detect the protein concentration. Then, 5× sodium dodecyl sulfate-polyacrylamide gel electrophoresis loading buffer was mixed with the protein sample at a ratio of 1:4 with heating for denaturation. Equal amounts of protein in each sample were resolved by sodium dodecyl sulfate-polyacrylamide gel electrophoresis and transferred onto a polyvinylidene fluoride membrane. Membranes were incubated with the primary antibody diluted with 5% bovine serum albumin-TBST at 4°C overnight. After three washes with TBST buffer, the blots were incubated with the secondary antibody (Abcam, Cambridge, UK) for 1 h at room temperature. β-actin was used as the internal reference protein. An automatic chemiluminescence image analysis system was used to develop and fix the images.

2.12.2 Real-time PCR

First, the myocardial tissue of rats was snap-frozen in liquid nitrogen, ground into a powder, and homogenized under RNase-free conditions. The total RNA was extracted from myocardial tissues using TRIzol reagent, and then RNA isolation and real-time PCR assay were conducted following the manufacturer's instructions.

2.12.3 Hematoxylin & eosin staining

Myocardial tissue samples were fixed in 10% formalin for 24 h and paraffin-embedded, and a microtome (Leica, Germany) was used to prepare 5-μm-thick sections. After drying overnight at 40°C, the sections were stained with hematoxylin & eosin.

2.12.4 Observation of the myocardial ultrastructure

The rat myocardial tissue was extracted, and a 1 mm3 section of tissue in the left ventricular anterior wall was taken at ligature 3 mm toward the apical direction, placed in 2.5% glutaraldehyde for pre-fixation for 2–4 h, rinsed with 0.1 M phosphate buffered saline, subjected to gradient dehydration, soaked, embedded, sliced using an ultrathin microtome (to approximately 60–80 nm), and finally double-stained with 2% uranium acetate saturated aqueous solution and lead citrate. The myocardial ultrastructures were observed under an H-600 transmission electron microscope (Hitachi Ltd., Tokyo, Japan).

2.12.5 ELISA

Interleukin (IL)-1α, IL-1β, IL-18, IL-33, IL-6, tumor necrosis factor (TNF)-α, and macrophage cationic peptide 1 (MCP-1) levels were measured using ELISA kits.

2.12.6 Statistical analysis

Data were presented as the mean ± SD and analyzed using Graph Pad Prism 6 (Graph Pad Software, Inc., La Jolla, CA, USA). Statistical analyses were performed using one-way ANOVA for group comparisons, and $P < 0.05$ was considered statistically significant.

3 Results

3.1 Treatment with SL improved survival and attenuated tissue damage in UFP-MII rats

The results of 2, 3, 5-triphenyltetrazolium chloride staining of the hearts are presented in Figure 1. Significantly greater cardiovascular damage was observed in the UFP-MI model group than in the sham operation group, whereas cardiovascular injury was significantly alleviated in the SLL and SLM group. The corresponding quantitative data are presented in Figure 1A, B.

The ultrastructure of rat myocardial tissue was observed via transmission electron microscopy (Figure 1C). Animals in the UFP-MI model group exhibited swelling of cardiac muscle myofilaments, mitochondrial swelling, the disappearance of mitochondrial cristae, and vacant areas. After treatment, the cellularity of myofilament sarcomeres was improved, and other observations included a compact arrangement, a clear Z-line, and mild swelling of some mitochondria.

The results of hematoxylin & eosin staining illustrated that in the sham group, the myocardial cells were neatly arranged, the myocardial fibers were regularly arranged, and there was no obvious inflammatory cell infiltration. In the model group, the arrangement of myocardial fibers was obviously disordered. Part of the tissue exhibited fibrous edema, the number of myocardial fibers between the gaps was increased, and local visible connective tissue hyperplasia accompanied by inflammatory cell infiltration was present. SL treatment significantly reduced myocardial damage, myocardial fibrosis, inflammatory cell infiltration, and myocardial structure damage. It was speculated that SL may exert its effects by mediating inflammation, and its possible anti-inflammatory mechanism was explored using transcriptomics and network pharmacology.

3.2 Transcriptomic analysis of differentially expressed genes (DEGs)

To address the system-wide mechanism of the effects of SL in UFP-MII rats, we performed transcriptomic analysis of myocardial tissue. We identified 778 DEGs in the model group, including 448 upregulated and 330 downregulated genes. Conversely, 337 DEGs were identified in the SL group, including 257 upregulated and 80 downregulated genes. By comparing the DEGs between the model and SL groups, the expression of 140 downregulated genes and 46 upregulated genes in the model group were altered by SL treatment (which we termed callback genes). The expression of most DEGs returned to normal, whereas a few genes remained upregulated.

3.3 Enrichment analysis of callback genes

Next, the interaction relationships among the 186 callback genes were identified using STRING, and these genes were subsequently analyzed using ClusterONE of Cytoscape 3.6.0 (as presented in Figure 2). Callback genes were mainly divided into three clusters. Cluster 1 genes were mainly involved in the biological processes of cell cycle, cell division, proliferation, and apoptosis. Cluster 2 genes were mainly enriched for innate immunity, type I interferon regulation, inflammatory response, and response to virus. Cluster 3 was enriched for a large number of inflammatory factors, such as C-C motif chemokine ligand 20 (CCL20), C-X-C motif chemokine ligand 10(CXCL10), and inflammatory cytokine interleukin-6 (IL-6), the biological process of which are mainly related to inflammation, immune regulation, response to lipopolysaccharide, and chemokines.

An analysis of callback genes also confirmed that SL had significant anti-inflammatory, immunomodulatory, and anti-viral effects. To further explore the potential anti-inflammatory and immunoregulatory mechanisms of SL in the treatment of UFP-MII, we first performed transcriptome sequencing and then searched for drug targets related to SL and disease targets related to particulate matter and CVD using network pharmacology.

3.4 Prediction of the candidate targets of SL and particulate matter and CVD targets

In the TCMIP V2.0 target prediction and functional analysis, using a similarity score of ≥0.8, 261 potential targets of the chemical components of *Salvia miltiorrhiza Bunge* and 117 potential targets of *Andrographis paniculata*（*Burm. f.*）*Nees* were obtained. After eliminating the repeated targets, 283 potential targets of SL were obtained. Regarding CVD genes were collected from TTD (2398 genes), DisGeNET (3240 genes), HPO (1018 genes), and pathogenic targets associated with CVD and particulate matter from research articles (509 genes), a total of 778 DEGs were identified in the transcriptome study. Finally, we selected data from research articles and transcriptome experiments to further construction a network based on their high reliability, and the number of genes was similar to that of drug targets. After eliminate the repeated targets, we obtained 1275 disease targets.

3.5 Candidate target network construction and enrichment analysis of SL

After constructing the database targets network diagram of SL, we explored its pharmacodynamics mechanism. The network consisted of 143 nodes and 1048 edges. Combined with the analysis function of the Cytoscape 3.6.0 ClusterONE module, the network was mainly divided into six clusters ($P \leq 0.05$). Then, we used BINGO to perform functional module analysis, and the results are presented in Figure 3. The biological function of cluster 1 was mainly involved in ATP biosynthesis and aerobic respiration. Cluster 2 was mainly enriched for cellular response to histamine, GABA-gated chloride ion channel activity, and ion transport. Cluster 3 genes were mainly involved in protein hydroxylation and procollagen–proline dioxygenase activity. Cluster 4 genes mainly regulated inflammatory response, apoptotic process, innate immune response, and platelet activation. The biological functions of cluster 5 were mainly regulation of hormone secretion. Cluster 6 was enriched for the regulation of coagulation.

3.6 Enrichment analysis and target–pathway network construction of SL for treating UFP-MII

The targets map of the core network of the candidate targets of SL and disease targets were constructed using PPI modules. By calculating the topological characteristic values of the nodes, screening, and assessing key hub node network targets, we obtained 93 core targets, including 30 genes identified in our transcriptome experiments (Figure 4). In the pathway enrichment analysis of the 93 core targets (Figure 4B, 4C), the results revealed their significant involvement in inflammatory and immune pathways, respiratory diseases, infectious diseases, and cardiovascular regulation. Among them, inflammatory immune pathways were mainly enriched for the Toll-like receptor signaling pathway, TNF signaling pathway, chemokine signaling pathway, NOD-like receptor signaling pathway, NF-κB signaling pathway, RIG-I-like receptor signaling pathway, and complement and coagulation cascades. NOD-like and RIG-I-like receptor signaling pathways were mainly involved in the regulation of the immune system (Figure 4E). A single enrichment analysis of 30 transcriptome genes among core targets revealed that these targets were mainly involved in two functional processes, namely cell cycle division and proliferation and immune regulation (Figure 4D).

Prolonged inflammation has been recognized as an underlying mechanism for many chronic diseases including cancer and CVD. Air pollution represents one of the most well-known causes of prolonged inflammation, and it eventually leads to innate immune system hyperactivation. The network enrichment analysis revealed that the core targets of SL in UFP-MI were also mainly the regulation of inflammation and immunity. Further transcriptomic analyses revealed that SL may exert anti-inflammatory effects by acting on the NOD-like signaling pathway to regulate immune response activation and inhibit systemic inflammatory development. Next, we used a variety of experimental methods to test this hypothesis.

3.7 Experimental validation

3.7.1 SL profoundly alleviates heart inflammation in rats with UFP-MI

Compared with the findings in the sham group, serum tumor necrosis factor (TNF-α) level was unchanged in the model group. However, IL-6, and monocyte chemoattractant protein-1(MCP-1) levels were significantly reduced in the model group. Compared with the findings in model group, serum TNF-α, IL-6, and MCP-1 levels in rats were significantly reduced by SL treatment. In addition, we found that the serum levels of IL-1α, IL-18, and IL-33 were all significantly increased in the model group, and the upregulation of IL-1α, IL-1β, IL-18, and IL-33 was reversed by SL treatment, as shown in Figure 5. Together, these data demonstrated that SL profoundly alleviated heart inflammation in rats with UFP-MI.

3.7.2 Inhibitory effects of SL on NLRP3 inflammasome activation

The expression of NLRP3 (NLR family pyrin domain containing 3), ASC (PYD and CARD domain containing), and Caspase-1 in rat myocardial tissue was detected using Western blotting to investigate the mechanism of action of SL against UFP-MI. As presented in Figure 6, the NLRP3 inflammasome was activated in the model group. Compared with the model group findings, NLRP3, ASC, and caspase-1 expression in myocardial tissue was significantly reduced by SL treatment. Meanwhile, the mRNA levels of NLRP3, ASC, and caspase-1 in rat myocardial tissue were significantly lower in the SL group than in the model group.

4 Discussion

The components of particulate matter are complex, and some toxic components reported in the literature mainly include chemical (e.g., polycyclic aromatic hydrocarbons, heavy metals), and biological components (e.g., bacteria, fungi, viruses, pollens, other microorganisms and their fragments) [29]. The current findings [30] indicate that fine Particles as foreign particles in the body can trigger inflammatory responses in affected organs. Alveolar macrophages or epithelial cells exposed to airborne particles release pro-inflammatory mediators and elevate circulating levels of TNF-α, IL-8, and IL-6, consistent with the possibility that the release of cytokines can trigger and sustain a state of mild systemic inflammation [31, 32]. Exposure to diesel exhaust particulate matter results in a markedly different response pattern. After exposure to a lower total dose for 6–18, neutrophilia, lymphocytosis, and mastocytosis were clearly present, resulting in bronchial mucosal damage, widespread inflammation, and adverse cardiovascular consequences [33]. The biological components of particulate matter, because of their specific ligand characteristics, have a unique “advantage” in activating the immune system and triggering an inflammatory response. The cell walls of gram-negative bacteria contain endotoxins (lipopolysaccharide) that contribute to the inflammatory effects of both coarse and fine particle air pollution [34]. Endotoxins can also stimulate localized or systemic inflammation via the activation of pattern recognition receptors [35]. Several studies reported that the biological and chemical components of particulate matter have synergistic pro-inflammatory effects [36-40].Some researchers have proven that particulate matter is a key cause of cardiovascular morbidity and mortality [41]. Animal experiments have also confirmed that particulate matter exposure triggers inflammation and oxidative stress, which may cause lung and heart injure [42, 43]. The potential pathophysiological mechanisms include inflammatory dysfunction, oxidative stress, abnormal activation of the hemostatic system, and disturbance of the autonomic nervous system [44-46]. Inflammation plays an important role in the development of chronic diseases [47]. Strong evidence of the association of particulate exposure with heart rate variability and systemic inflammation has been published [48].

The intracellular pattern recognition NOD receptor family member NLRP3 may be a key molecule that senses particulate matter-induced damage signals and triggers the inflammatory response [49,50]. NLRP3 can instantly activate innate immune cells to respond to dangerous and pathogen-associated molecules [51,52]. After NLRP3 is activated, the apoptosis-related particle proteins ASC and caspase-1 constitute the NLRP3 inflammasome, triggering the caspase-1–mediated release of IL-1β, IL-18, and IL-33 and initiating the inflammatory response [53].

Previous studies revealed that SL had significant inhibitory effects on IL-1 and IL-6 expression. SL can inhibit the inflammatory response of macrophages, and its mechanism may be related to an influence on the phenotypic transformation of macrophages, the secretion of M1 inflammatory factors, and activation of the NF-κB signaling pathway in macrophages [16,17, 18]. Another study reported that SL can significantly improve the imbalance of pro-inflammatory and pro-resolving mediators during atherosclerotic inflammation [54]. In addition, a number of studies found that *Salvia miltiorrhiza Bunge* [26, 27] and *Andrographis paniculata*（*Burm. f.*） *Nees* [55, 56, 57] had significant effects on inflammation and immune regulation.

Pharmacodynamic experiments proved that SL could effectively treat myocardial injury caused by UFPs and significantly improve the pathological state of the inflammatory infiltration of myocardial tissue. This indicates that SL can be used to treat particulate matter-induced myocardial ischemic damage; however, because of the "multi-component" and "multi-target" features of TCMs, it is difficult to study the mechanism of action using traditional methods. Therefore, we first conducted transcriptomic analysis of heart tissues before and after treatment and then added network pharmacology to gain insight into the pharmacological mechanism of SL in the treatment of UFP-MII. Functional enrichments of callback genes indicated that SL had significant anti-inflammatory, immunomodulatory, and anti-viral effects. Using network pharmacology to retrieve the drug targets of SL, the biological function enrichment analysis found that SL influenced the inflammatory response, apoptotic process, innate immune response, and platelet activation. Finally, we combined the transcriptomic results and network pharmacology data to further explore the potential anti-inflammatory mechanism of SL. The PPI network map of the candidate targets of SL and disease targets was constructed, and the core targets were selected. In total, 30 DEGs were identified among the core targets, and enrichment analysis of these genes revealed their involvement in regulation of the immune system. Pathway enrichment analysis of all core targets uncovered a large number of inflammation- and immune-related pathways. Thus, we speculated that SL may play an anti-inflammatory role by acting on the NOD-like signaling pathway to regulate immune response activation and inhibit systemic inflammatory development.

The NOD-like receptor family is a group of pattern recognition receptors, known to mediate the initial innate immune response to cellular injury and infection [58]. NLRP3 is a major inflammasome in CVD, and it belongs to the NOD-like receptor family. Inflammasomes are intracellular multi-protein complexes, and their components include NLRP3, ASC, and pro-caspase-1. Animal experiments [49,59, 60] illustrated that the downregulation of NLRP3, IL-1, and IL-18 can significantly reduce the area of infarction, inhibit NLRP3 inflammasome activation, and improve myocardial function. Prior studies [61] reported that particulate matter can activate the NLRP3 inflammasome. Du et al. [62] found that mononuclear macrophage (CD11c+) counts were significantly elevated in ApoE$^{-/-}$ mice exposed to fine particulate matter, and NLRP3, ASC, caspase-1, IL-1, and IL-18 expression was also increased. The results illustrated that fine particulate matter-related heart injury was mediated by macrophage polarization and NLRP3 inflammasome activation, in line with the current study results. The current data further demonstrated that SL inhibits the activation of the NLRP3 inflammasome in myocardial tissue and alleviate cytokine release into blood, thereby reduce systemic inflammation

Using through the combination of transcriptomic analysis and network pharmacology, the mechanism by which SL alleviates UFP-MI was uncovered. After constructing a series of PPI network diagrams, the potential targets and pathways of SL were screened, and their reliability was verified experimentally. NLRP3 and other related proteins were not enriched in the NOD-like signaling pathway in transcriptomics, which may be related to sample loading and protein sensitivity. However, in later validation experiments, the expression of NLRP3-related proteins was significantly changed by SL treatment. At present, only in vivo experiments have been conducted, and the corresponding verification will be conducted in the later stage of in vitro experimentation.

Further analysis of the mechanism of action demonstrated that the effects of SL are closely related to the RIG-I-like receptor signaling pathway, which is also a pattern recognition receptor. In addition, a large

number of genes involved in the regulation of this pathway were enriched in the transcriptome, which will also be verified by experiments in the later stage.

5 Conclusion

UFP can induce the activation of NLRP3 inflammasome, leading to the release of downstream the inflammatory cytokines, aggravate the pathological conditions of inflammatory infiltration, and further aggravate the myocardial ischemic injury. Experimental verification demonstrated that SL can directly inhibit the activation of the NLRP3 inflammasome in the NOD-like signaling pathway and reduce the release of IL-1 family cytokines. In conclusion, our results confirm that SL may prevent UFP-MI by acting on the NOD-like signaling pathway.

Abbreviations

SL: Shenlian extract ; UFP-MI: ultrafine particle-induced myocardial ischemic injury; CVD: cardiovascular disease; MI: ischemic injury; PAHs: polycyclic aromatic hydrocarbons; Nitro-PAHs: nitro-polycyclic aromatic hydrocarbons; LAD: left anterior descending coronary artery; PPI: protein–protein interaction; IL-1α: Interleukin-1α; IL-1β: Interleukin-1β, IL-18: Interleukin-18; Interleukin-33: IL-33; IL-6: interleukin-6; TNF- α: tumor necrosis factor-α; MCP-1: macrophage cationic peptide 1;DEGs differentially expressed genes; NLRP3: NLR family pyrin domain containing 3; CCL20: C-C motif chemokine ligand 20; CXCL10: C-X-C motif chemokine ligand 10.

Ethics Statement

All animals received human care throughout the experiments and the study protocols were approved by the Committee on the Use of Live Animals in Teaching and Research (CULATR). This study was performed according to the instructions of the Guide for the Care and Use of Laboratory Animals and the guidelines of Institute of Chinese Materia Medica Animal Research Committee.

Consent for publication

Not applicable

Availability of data and materials

All data generated or analysed during this study are included in this published article and its supplementary information files.

Competing interests

The authors declare that no competing interests.

Funding

This study was supported by the National Natural Science Foundation of China (No. 81673640, 81841001 and 81803814), Major National Science and Technology Program of China for Innovative Drug (2017ZX09301012002，2017ZX09101002-001-001-3).

Author Contributions

SQ contributed to the acquisition of data, the analysis and interpretation of the data and drafting of the work. KL, YY, TY, ZZ, HL, XW, YZ, SD conducted the experiments and analyzed data. YL, XZ, LC design of the study and revising the work.

Acknowledgments

Special thanks to Dr. Yanqiong Zhang for guidance and help in data analysis.

Affiliations

1 Artemisinin Research Center, China Academy of Chinese Medical Sciences, Beijing China.

2 Institute of Chinese Materia Medica, China Academy of Chinese Medical Sciences, Beijing China.

3 School of Tranditional Chinese Medicine，GDPU.

References

1. Zavala, J.; Freedman, A.N.; Szilagyi, J.T., et al. New Approach Methods to Evaluate Health Risks of Air Pollutants: Critical Design Considerations for In Vitro Exposure Testing. Int J Environ Res Public Health 2020, 17. doi: 10.3390/ijerph17062124.
2. Miller, M.R.; Newby, D.E. Air pollution and cardiovascular disease: car sick. Cardiovasc. Res. 2020, 116, 279-294.doi:10.1093/cvr/cvz228.
3. Raza, W.; Forsberg, B.; Johansson, C.; Sommar, J.N. Air pollution as a risk factor in health impact assessments of a travel mode shift towards cycling. Glob Health Action 2018, 11, 1429081. doi: 10.1080/16549716.2018.1429081.
4. Kotsyfakis, M.; Patelarou, E. MicroRNAs as biomarkers of harmful environmental and occupational exposures: a systematic review. Biomarkers 2019, 24, 623-630. doi: 10.1080/1354750X.2019.1652348.
5. Zhang, Y.; Wang, S.G.; Ma, Y.X., et al. Association between Ambient Air Pollution and Hospital Emergency Admissions for Respiratory and Cardiovascular Diseases in Beijing: a Time Series Study. Biomed. Environ. Sci. 2015, 28, 352-363. doi: 10.3967/bes2015.049.
6. Kwon, H.S.; Ryu, M.H.; Carlsten, C. Ultrafine particles: unique physicochemical properties relevant to health and disease. Exp. Mol. Med. 2020, 52, 318-328. doi: 10.1038/s12276-020-0405-1.
7. Khan, K.M.; Weigel, M.M.; Yonts, S.; Rohlman, D.; Armijos, R. Residential exposure to urban traffic is associated with the poorer neurobehavioral health of Ecuadorian schoolchildren. Neurotoxicology 2019, 73, 31-39. doi: 10.1016/j.neuro.2019.02.018.
8. Miller, M.R.; Raftis, J.B.; Langrish, J.P., et al. Inhaled Nanoparticles Accumulate at Sites of Vascular Disease. ACS Nano 2017, 11, 4542-4552. doi: 10.1021/acsnano.6b08551.
9. Lee, H.C.; Lin, T.H. Air Pollution Particular Matter and Atherosclerosis. Acta Cardiol Sin 2017, 33, 646-647. doi: 10.6515/ACS20170615A.
10. Yang, S.; Lee, S.P.; Park, J.B., et al. PM2.5 concentration in the ambient air is a risk factor for the development of high-risk coronary plaques. Eur Heart J Cardiovasc Imaging 2019, 20, 1355-1364. doi: 10.1093/ehjci/jez209.
11. Zhao, J.; Mi, X.; Zhao, L., et al. Validation of PM2.5 model particle through physicochemical evaluation and atherosclerotic plaque formation in ApoE-/- mice. Ecotoxicol. Environ. Saf. 2020, 192, 110308. 10.1016/j.ecoenv.2020.110308.
12. Rao, X.; Zhong, J.; Maiseyeu, A., et al. CD36-dependent 7-ketocholesterol accumulation in macrophages mediates progression of atherosclerosis in response to chronic air pollution exposure. Circ. Res. 2014, 115, 770-780. doi: 10.1161/CIRCRESAHA.115.304666.
13. Hartiala, J.; Breton, C.V.; Tang, W.H., et al. Ambient Air Pollution Is Associated With the Severity of Coronary Atherosclerosis and Incident Myocardial Infarction in Patients Undergoing Elective Cardiac Evaluation. J Am Heart Assoc 2016, 5. doi: 10.1161/JAHA.116.003947.

14. Guo, Y.; Liu, X.C.; Wang, Y.J., et al. Effects of Shenlian extract on experimental atherosclerosis in ApoE-deficient mice based on ultrasound biomicroscopy. BMC Complement Altern Med 2016, 16, 469. doi: 10.1186/s12906-016-1449-6.
15. Li Yu-jie, Ruan Cong-xiao, Yang Qing, et al. Establishment of vulnerable plaque model by mast cell activation in adventitia and evaluation of effectiveness of intervention of Shenlian tablet. Acta Pharmaceutica Sinica. 2016. 51(08): 1263-1270.
16. Liu Si-si, Li Qi, Sun Li-dong, et al. Effects of Shenlian Extract on Lipopolysaccharide-induced Inflammation of Macrophages. Chinese Journal of Experimental Traditional Medical Formulae. 2017. 23(10): 85-91.
17. Zhou Bing-bing, Li Yu-jie, Li Qi et al. Effect on M1 macrophages of Shenlian extracts. China Journal of Chinese Materia Medica. 2014. 39(11): 2086-2090.
18. Guo, Y.; Yang, Q.; Weng, X.G., et al. Shenlian Extract Against Myocardial Injury Induced by Ischemia Through the Regulation of NF-κB/IκB Signaling Axis. Front Pharmacol 2020, 11, 134. doi: 10.3389/fphar.2020.00134.
19. Chen, Y.; Kern, T.S.; Kiser, P.D.; Palczewski, K. Eyes on systems pharmacology. Pharmacol. Res. 2016, 114, 39-41. doi: 10.1016/j.phrs.2016.09.026.
20. Li, S.; Zhang, B. Traditional Chinese medicine network pharmacology: theory, methodology and application. Chin J Nat Med 2013, 11, 110-120. doi: 10.1016/S1875-5364(13)60037-0.
21. Guo, W.; Huang, J.; Wang, N., et al. Integrating Network Pharmacology and Pharmacological Evaluation for Deciphering the Action Mechanism of Herbal Formula Zuojin Pill in Suppressing Hepatocellular Carcinoma. Front Pharmacol 2019, 10, 1185. doi: 10.3389/fphar.2019.01185.
22. Li Yu-jie, Zhu Xiao-xin, Yang qing, et al.(2011) Effect of Salviae Miltiorhize Radix and Andrographitis Herba extracts on vessel pathological changes and lipid metabolism in artherosclerosis rabbits. Chinese Traditional and Herbal Drugs. 2011. 42(04): 760-764.
23. Zhang, X.; Guan, J.; Guo, M., et al. Rho GTPase-activating protein 1 promotes apoptosis of myocardia1 cells in an ischemic cardiomyopathy model. Kardiol Pol 2019, 77, 1163-1169. doi: 10.33963/KP.15040.
24. Xu, H.Y.; Zhang, Y.Q.; Liu, Z.M., et al. ETCM: an encyclopaedia of traditional Chinese medicine. Nucleic Acids Res. 2019, 47, D976-976D982. doi: 10.1093/nar/gky987.
25. Cui Ru-yi, Xu Hai-yu. Study on quality markers of ginseng acting on heart failure based on TCMIP V2.0. Chinese Traditional and Herbal Drugs. 2019. 50(19): 4628-4633.
26. Zhang Qian-tao, Hou min-na, Peng Xiu-juan, et al. The predictive analysis of action mechanism for classic TCM excellent prescriptions of Danggui Buxue decoction on diabetes with TCMIP. Chinese Pharmacological Bulletin. 2019. 35(09): 1314-1319.
27. Xu, H.Y.; Liu, Z.M.; Fu, Y., et al. Exploiture and application of an internet-based Computation Platform for Integrative Pharmacology of Traditional Chinese Medicine. Zhongguo Zhong Yao Za Zhi 2017, 42, 3633-3638. doi: 10.19540/j.cnki.cjcmm.2017.0141.
28. Xie, G.; Peng, W.; Li, P., et al. A Network Pharmacology Analysis to Explore the Effect of Astragali Radix-Radix Angelica Sinensis on Traumatic Brain Injury. Biomed Res Int 2018, 2018, 3951783. doi: 10.1155/2018/3951783.
29. Wang Zhi-hong. Studies on the pro-inflammatory effects of atmospheric particulate matter biochemical components. Chemical Enterprise Management. 2020. (12): 19-20.
30. Yoshizaki, K.; Brito, J.M.; Toledo, A.C., et al. Subchronic effects of nasally instilled diesel exhaust particulates on the nasal and airway epithelia in mice. Inhal Toxicol 2010, 22, 610-617. doi: 10.3109/08958371003621633.

564 31. Pope, C.A.; Bhatnagar, A.; McCracken, J.P.; Abplanalp, W.; Conklin, D.J.; O'Toole, T. Exposure to Fine
565 Particulate Air Pollution Is Associated With Endothelial Injury and Systemic Inflammation. Circ. Res.
566 2016, 119, 1204-1214. doi: 10.1161/CIRCRESAHA.116.309279.
567 32. Siponen, T.; Yli-Tuomi, T.; Aurela, M., et al. Source-specific fine particulate air pollution and systemic
568 inflammation in ischaemic heart disease patients. Occup Environ Med 2015, 72, 277-283. doi:
569 10.1136/oemed-2014-102240.
570 33. Sehlstedt, M.; Dove, R.; Boman, C., et al. Antioxidant airway responses following experimental
571 exposure to wood smoke in man. Part Fibre Toxicol 2010, 7, 21. doi: 10.1186/1743-8977-7-21.
572 34. Behbod, B.; Urch, B.; Speck, M., et al. Endotoxin in concentrated coarse and fine ambient particles
573 induces acute systemic inflammation in controlled human exposures. Occup Environ Med 2013, 70,
574 761-767. doi: 10.1136/oemed-2013-101498.
575 35. Mani, V.; Weber, T.E.; Baumgard, L.H.; Gabler, N.K. Growth and Development Symposium: Endotoxin,
576 inflammation, and intestinal function in livestock. J. Anim. Sci. 2012, 90, 1452-1465. doi:
577 10.2527/jas.2011-4627.
578 36. Liu, D.; Mariman, R.; Gerlofs-Nijland, M.E., et al. Microbiome composition of airborne particulate
579 matter from livestock farms and their effect on innate immune receptors and cells. Sci. Total Environ. 2019,
580 688, 1298-1307. doi: 10.1016/j.scitotenv.2019.06.217.
581 37. Liu, Q.; Baumgartner, J.; Schauer, J.J. Source Apportionment of Fine-Particle, Water-Soluble Organic
582 Nitrogen and Its Association with the Inflammatory Potential of Lung Epithelial Cells. Environ. Sci.
583 Technol. 2019, 53, 9845-9854. doi: 10.1021/acs.est.9b02523.
584 38. Brinchmann, B.C.; Skuland, T.; Rambøl, M.H., et al. Lipophilic components of diesel exhaust particles
585 induce pro-inflammatory responses in human endothelial cells through AhR dependent pathway(s). Part
586 Fibre Toxicol 2018, 15, 21. doi: 10.1186/s12989-018-0257-1.
587 39. Baulig, A.; Singh, S.; Marchand, A., et al. Role of Paris PM(2.5) components in the pro-inflammatory
588 response induced in airway epithelial cells. Toxicology 2009, 261, 126-135. doi: 10.1016/j.tox.2009.05.007.
589 40. Xiao, G.G.; Wang, M.; Li, N.; Loo, J.A.; Nel, A.E. Use of proteomics to demonstrate a hierarchical
590 oxidative stress response to diesel exhaust particle chemicals in a macrophage cell line. J. Biol. Chem. 2003,
591 278, 50781-50790. doi: 10.1074/jbc.M306423200.
592 41. Brook, R.D.; Rajagopalan, S.; Pope, C.A., et al. Particulate matter air pollution and cardiovascular
593 disease: An update to the scientific statement from the American Heart Association. Circulation 2010, 121,
594 2331-2378. doi: 10.1161/CIR.0b013e3181dbece1.
595 42. Jiang, S.; Bo, L.; Du X, et al. CARD9-mediated ambient PM2.5-induced pulmonary injury is associated
596 with Th17 cell. Toxicol. Lett. 2017, 273, 36-43. doi: 10.1016/j.toxlet.2017.03.015.
597 43. Zhao, J.; Liu, C.; Bai, Y.; Wang, T.Y.; Kan, H.; Sun, Q. IKK inhibition prevents PM2.5-exacerbated cardiac
598 injury in mice with type 2 diabetes. J Environ Sci (China) 2015, 31, 98-103. doi: 10.1016/j.jes.2014.10.018.
599 44. Feng, S., Gao, D., Liao, F., Zhou, F., and Wang, X. The health effects of ambient PM2.5 and potential
600 mechanisms. Ecotoxicol. Environ. Saf. 128, 67-74. doi: 10.1016/j.ecoenv.2016.01.030
601 45. Wang, C.; Tu, Y.; Yu, Z.; Lu, R. PM2.5 and Cardiovascular Diseases in the Elderly: An Overview. Int J
602 Environ Res Public Health 2015, 12, 8187-8197. doi: 10.3390/ijerph120708187.
603 46. Lawal, A.O. Air particulate matter induced oxidative stress and inflammation in cardiovascular disease
604 and atherosclerosis: The role of Nrf2 and AhR-mediated pathways. Toxicol. Lett. 2017, 270, 88-95. doi:
605 10.1016/j.toxlet.2017.01.017.

606 47. Shou, Y.; Zhu, X.; Zhu, D., et al. Ambient PM2.5 chronic exposure leads to cognitive decline in mice:
607 From pulmonary to neuronal inflammation. Toxicol. Lett. 2020, 331, 208-217. doi:
608 10.1016/j.toxlet.2020.06.014.
609 48. Fang, S.C.; Cassidy, A.; Christiani, D.C. A systematic review of occupational exposure to particulate
610 matter and cardiovascular disease. Int J Environ Res Public Health 2010, 7, 1773-1806. doi:
611 10.3390/ijerph7041773.
612 49. Du X; Jiang, S.; Zeng, X., et al. Fine particulate matter-induced cardiovascular injury is associated with
613 NLRP3 inflammasome activation in Apo E-/- mice. Ecotoxicol. Environ. Saf. 2019, 174, 92-99. doi:
614 10.1016/j.ecoenv.2019.02.064.
615 50. Ding, S.; Wang, H.; Wang, M.; Bai, L.; Yu, P.; Wu, W. Resveratrol alleviates chronic "real-world" ambient
616 particulate matter-induced lung inflammation and fibrosis by inhibiting NLRP3 inflammasome
617 activation in mice. Ecotoxicol. Environ. Saf. 2019, 182, 109425. doi: 10.1016/j.ecoenv.2019.109425.
618 51. Li, H.; Zhang, S.; Li, F.; Qin, L. NLRX1 attenuates apoptosis and inflammatory responses in myocardial
619 ischemia by inhibiting MAVS-dependent NLRP3 inflammasome activation. Mol. Immunol. 2016, 76,
620 90-97. doi: 10.1016/j.molimm.2016.06.013.
621 52. Toldo, S.; Marchetti, C.; Mauro, A.G., et al. Inhibition of the NLRP3 inflammasome limits the
622 inflammatory injury following myocardial ischemia-reperfusion in the mouse. Int. J. Cardiol. 2016, 209,
623 215-220. doi: 10.1016/j.ijcard.2016.02.043.
624 53. Shi, J.; Gao, W.; Shao, F. Pyroptosis: Gasdermin-Mediated Programmed Necrotic Cell Death. Trends
625 Biochem. Sci. 2017, 42, 245-254. doi: 10.1016/j.tibs.2016.10.004.
626 54. Guo Y. Mechanism study of Shenlian extract on the regulation of atherosclerotic inflammation
627 resolution. (11), 2015.
628 55. Lin Meng-ya, Zhang Yu-ping, Li Ya, et al. Spectra-effect relationship of anti-inflammation of Salvia
629 miltiorrhiza extract based on gray correlation analysis. Chinese Traditional and Herbal Drugs 48,
630 3447-3452. doi: 10.7501/j.issn.0253-2670.2017.16.031.
631 56. Wang Han, Yang Na, Tan jing, et al. Research Progress on Salvia Miltiorrhiza Bge of the Chemical
632 Constituents and Their Pharmacological Effects. Special Wild Economic Animal and Plant Research. 2018.
633 40(1): 48-53.
634 57. Yin Qing, Deng Ming-ming. Progress in research on anti-inflammatory mechanism of Andrographolide.
635 Guangdong Medical Journal. 2014. 35(5): 786-788.
636 58. Tong jiao, Ge Zi-yu, Jiang Li. Progress in the study of in vivo distribution and anti-inflammatory
637 mechanism of andrographolide and its derivatives. Chinese Journal of Clinical Rational Drug Use 2020,
638 13, 180-181. doi: 10.15887/j.cnki.13-1389/r.2020.08.107.
639 59. Lamkanfi, M.; Dixit, V.M. Mechanisms and functions of inflammasomes. Cell 2014, 157, 1013-1022. doi:
640 10.1016/j.cell.2014.04.007.
641 60. Liu, Y.; Lian, K.; Zhang, L., et al. TXNIP mediates NLRP3 inflammasome activation in cardiac
642 microvascular endothelial cells as a novel mechanism in myocardial ischemia/reperfusion injury. Basic
643 Res. Cardiol. 2014, 109, 415. doi: 10.1007/s00395-014-0415-z.
644 61. van Hout GP; Arslan, F.; Pasterkamp, G.; Hoefer, I.E. Targeting danger-associated molecular patterns
645 after myocardial infarction. Expert Opin. Ther. Targets 2016, 20, 223-239. doi:
646 10.1517/14728222.2016.1088005.
647 62. Yan, Z.; Jin, Y.; An, Z.; Liu, Y.; Samet, J.M.; Wu, W. Inflammatory cell signaling following exposures to
648 particulate matter and ozone. Biochim. Biophys. Acta 2016, 1860, 2826-2834. doi:
649 10.1016/j.bbagen.2016.03.030.

650 **Figures**

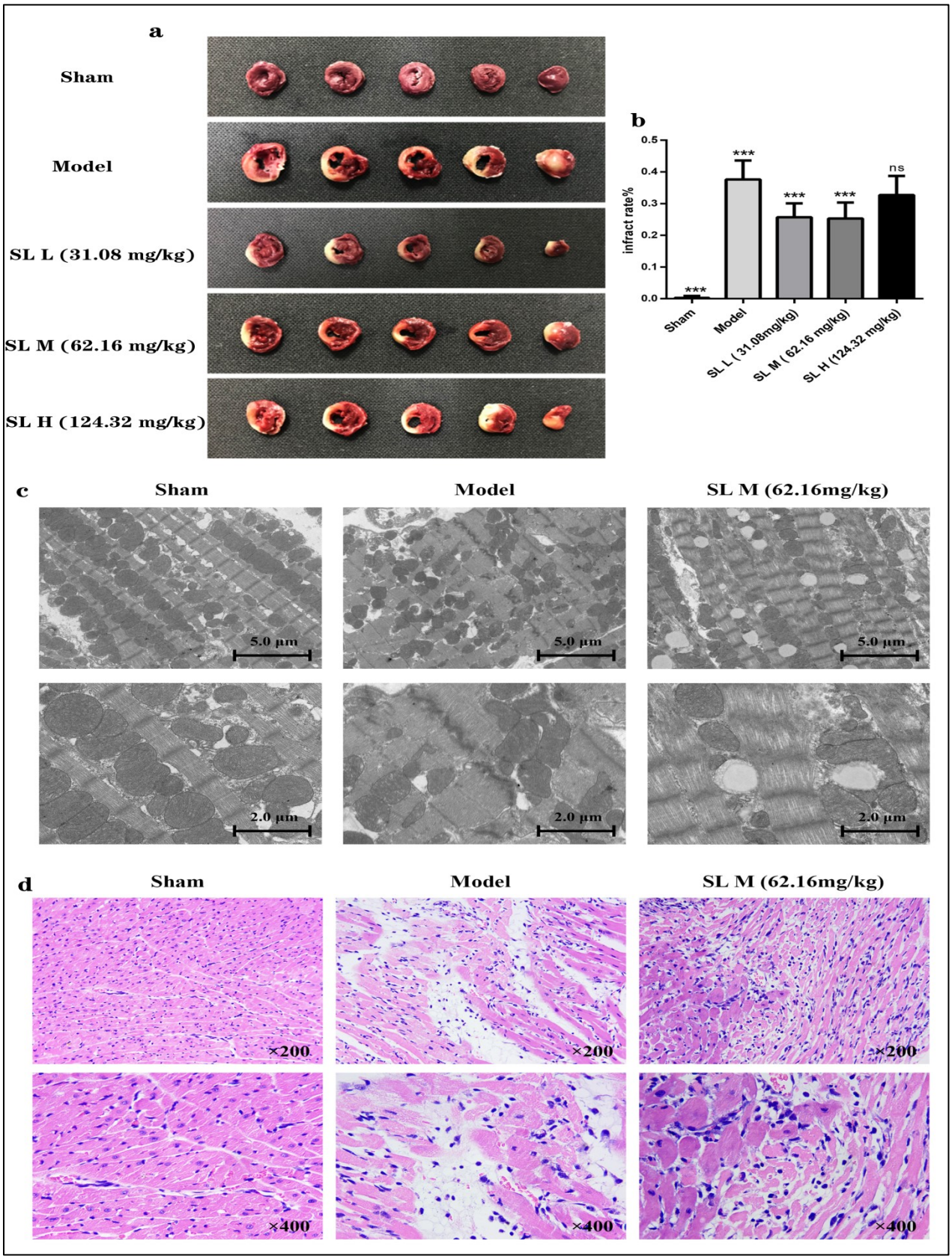

651

652 **Figure 1.** Efficacy evaluation of Shenlian extract (SL). (a, b) Effect of SL on infarct size in the experimental
653 rats and the infarct rate as a percentage of the total size. Heart sections of the experimental rats stained
654 with 2, 3, 5-triphenyltetrazolium chloride. Normal tissue was stained red, and infarcted tissue was pale. (c)

Ultrastructural changes of myocardial tissue and the effect of SL treatment (left, ×2000; right, ×50,000). (d) Myocardial histopathological changes and SL in rats (hematoxylin & eosin: left, ×200; right, ×400). *P < 0.05, **P < 0.01, ***P < 0.001.

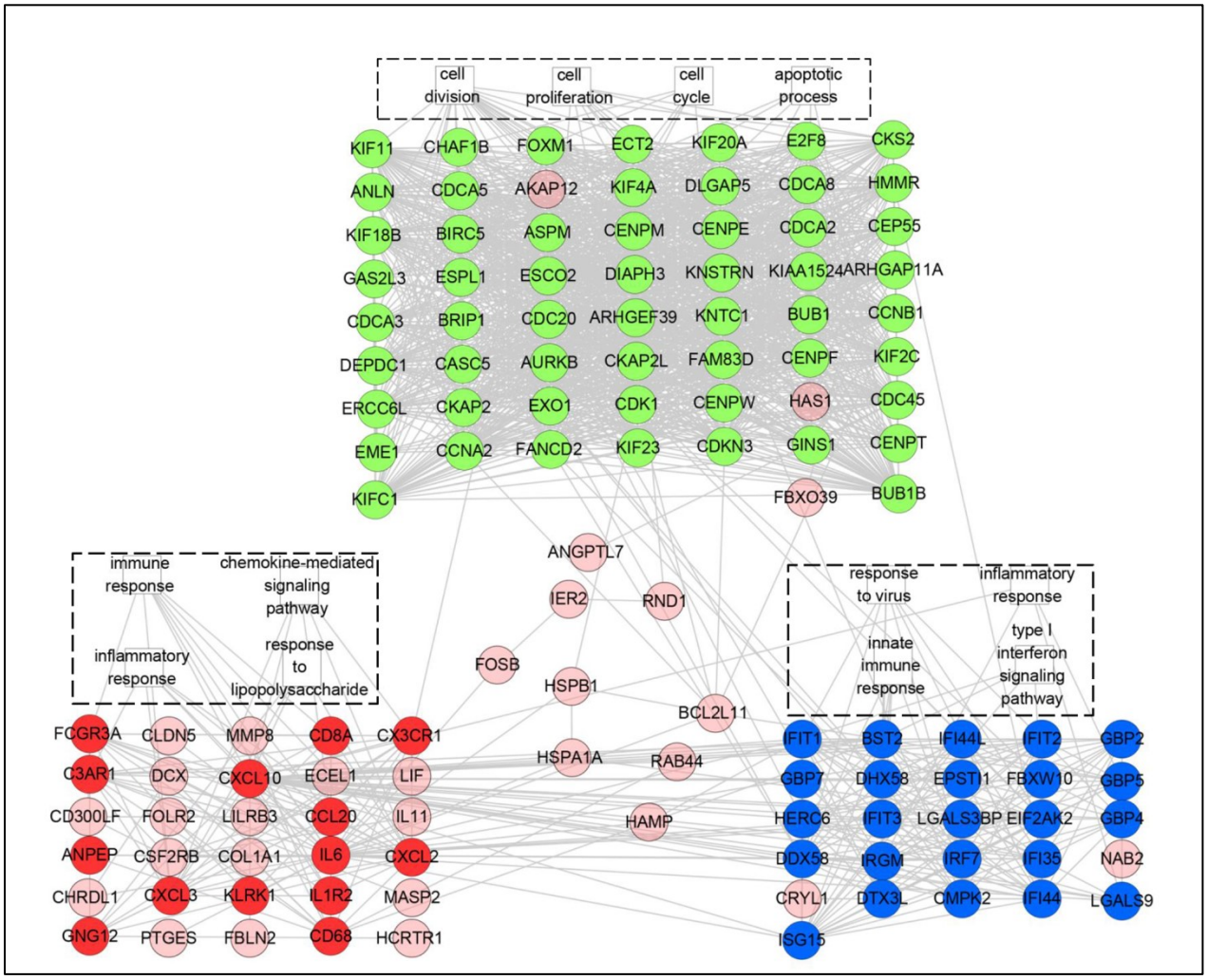

Figure 2. The enrichment analysis of genes altered by SL treatment following ultrafine particle-induced myocardial ischemic injury. The green, blue, and red nodes represent clusters 1, 2, and 3, respectively, and the pink nodes are the join points.

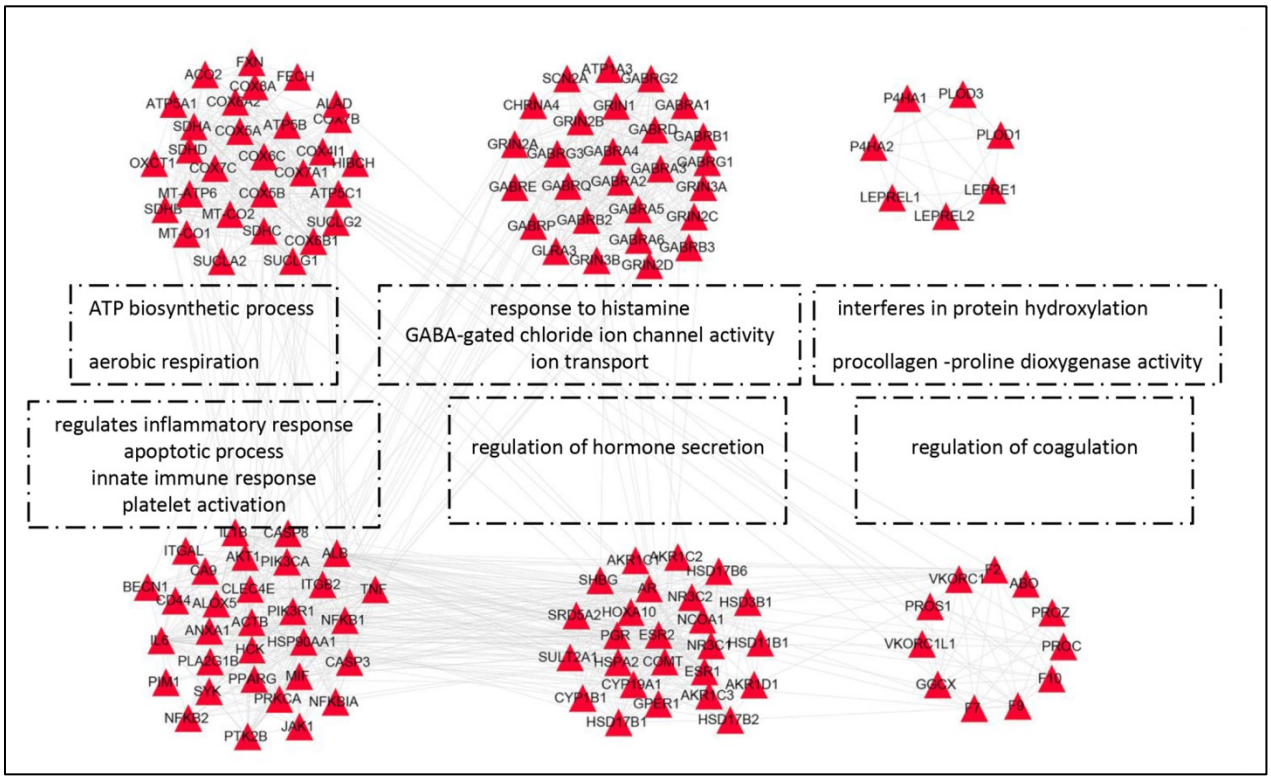

662

663 **Figure3.** Enrichment analysis of Shenlian extract (SL). From top to bottom and from left to right, six
664 clusters are respectively represented. The red triangles denote SL compound target, and the dashed boxes
665 denote the biological function involving the corresponding cluster targets.

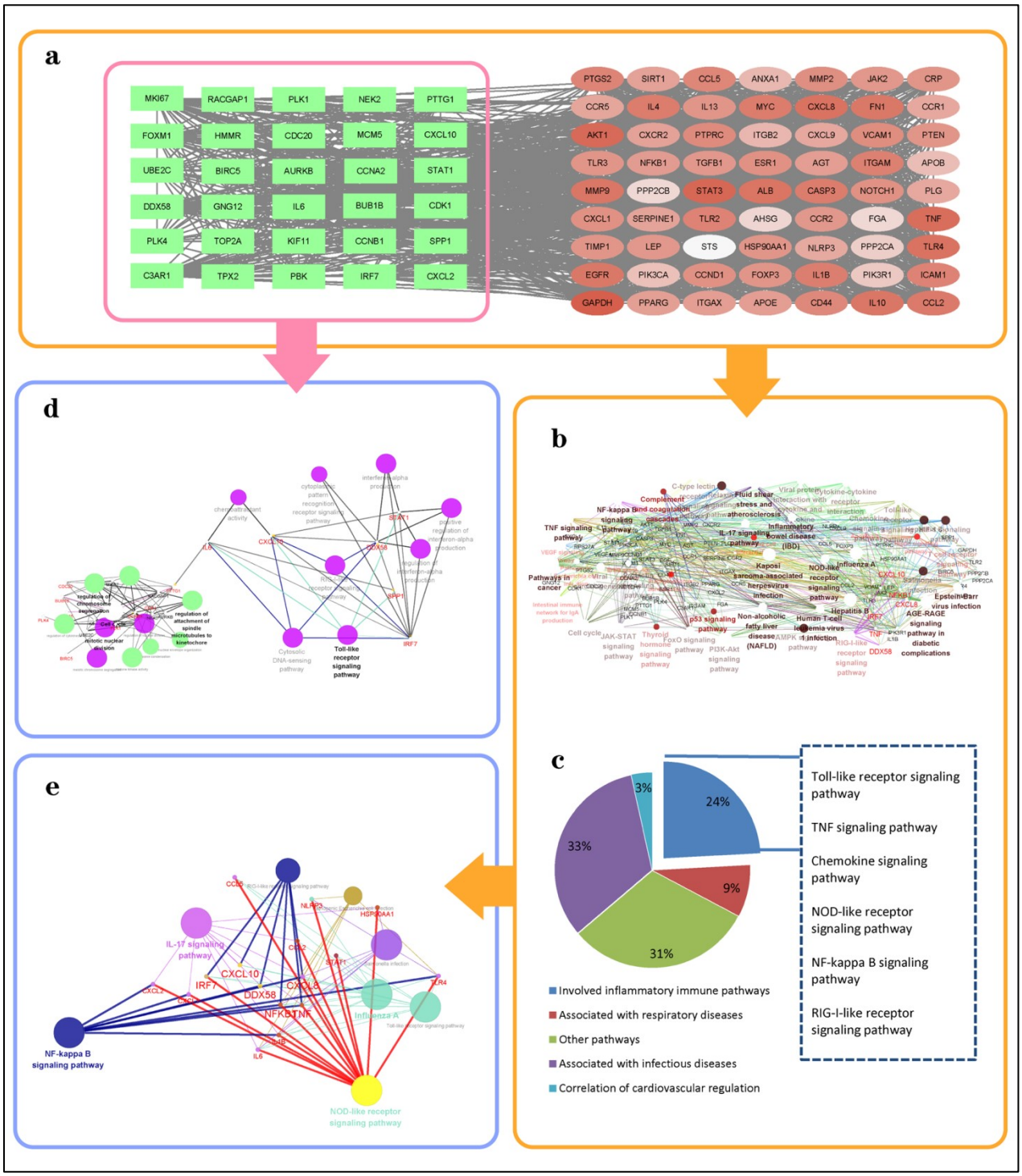

Figure 4. Enrichment analysis and target–pathway network construction for Shenlian extract for treating ultrafine particle-induced myocardial ischemic injury (a) Ninety-three core targets, including 30 green genes identified by our transcriptome research. (b, c) Pathway enrichment analysis of the 93 core targets. (d) The enrichment analysis of 30 transcriptome genes among core targets. (e) Key pathways of core target enrichment.

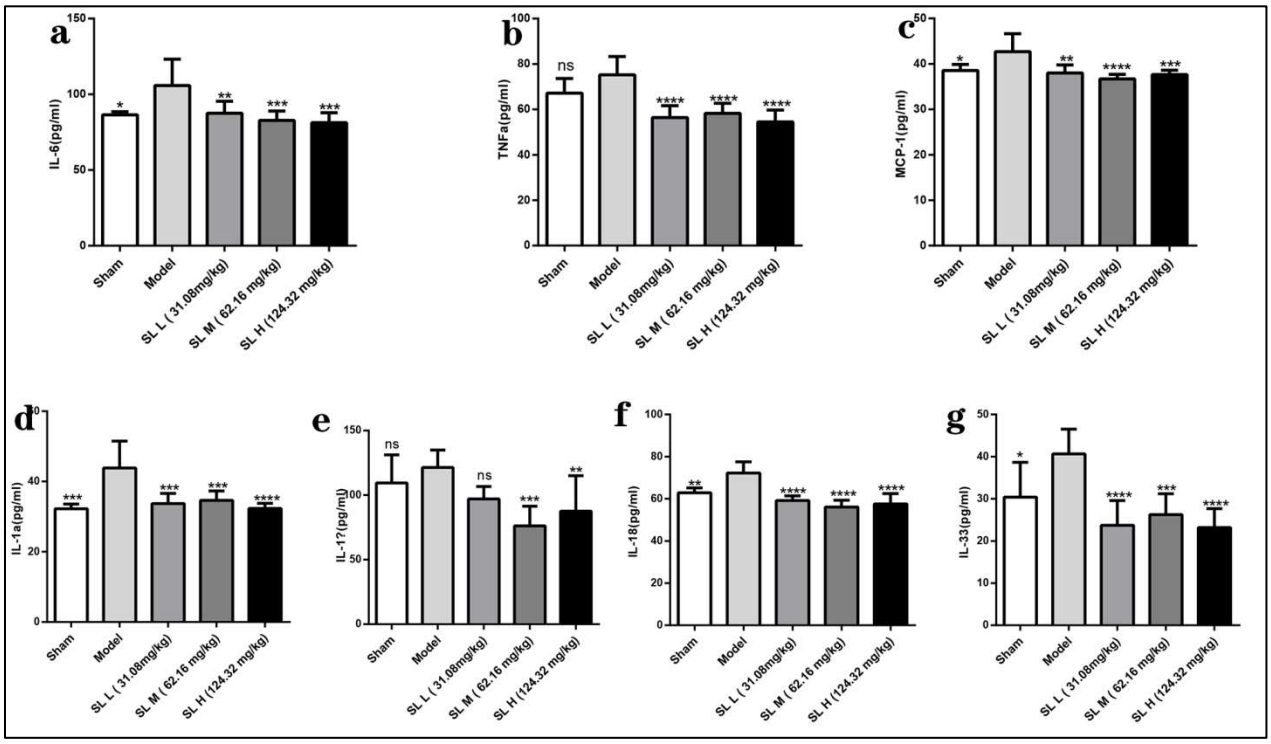

672

673 **Figure 5.** Expression of inflammatory factors and NLRP3 inflammasome-associated downstream
674 cytokines. (a-c) The changes of inflammatory cytokine interleukin (IL)-6, tumor necrosis factor (TNF)-α,
675 monocyte chemoattractant protein-1 (MCP)-1 levels in the serum of rats and the effects of Shenlian extract
676 (SL). (d-g) Quantitative reverse results of interleukin (IL)-1α, IL-1β, IL-18, and IL-33 in the serum of rats.
677 *P < 0.05, **P < 0.01, ***P < 0.001,****P < 0.0001.

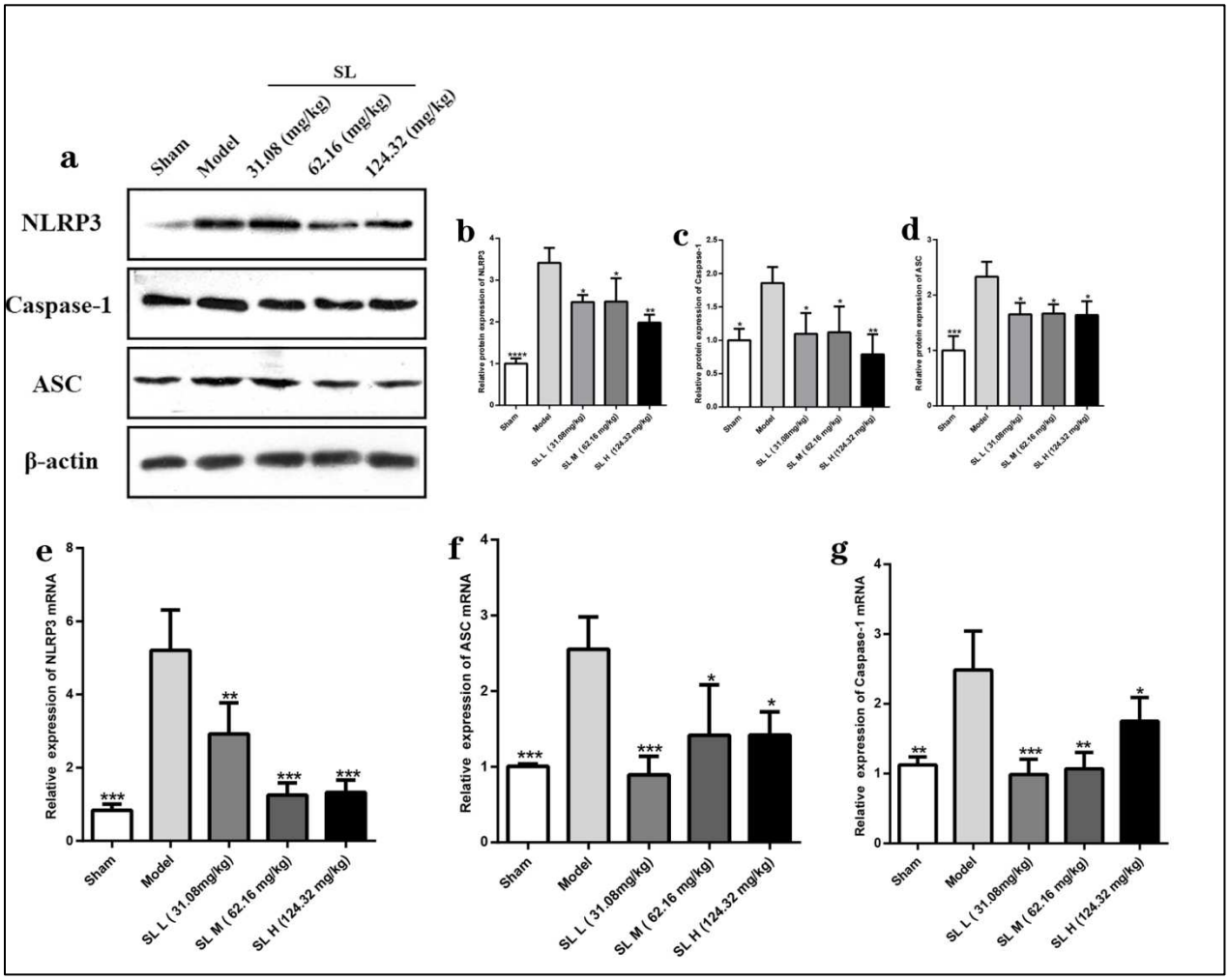

678

679 **Figure 6.** The expression of NLRP3 inflammasome. (a- d) Expression of NLRP3 inflammasome-associated
680 proteins in the myocardial tissue of rats (n = 3, x ± s). (e-g) Expression of NLRP3 inflammasome-associated
681 mRNA in the myocardial tissue of rats (n = 3, x ± s). *P < 0.05, **P < 0.01, ***P < 0.001.

682

683

Figures

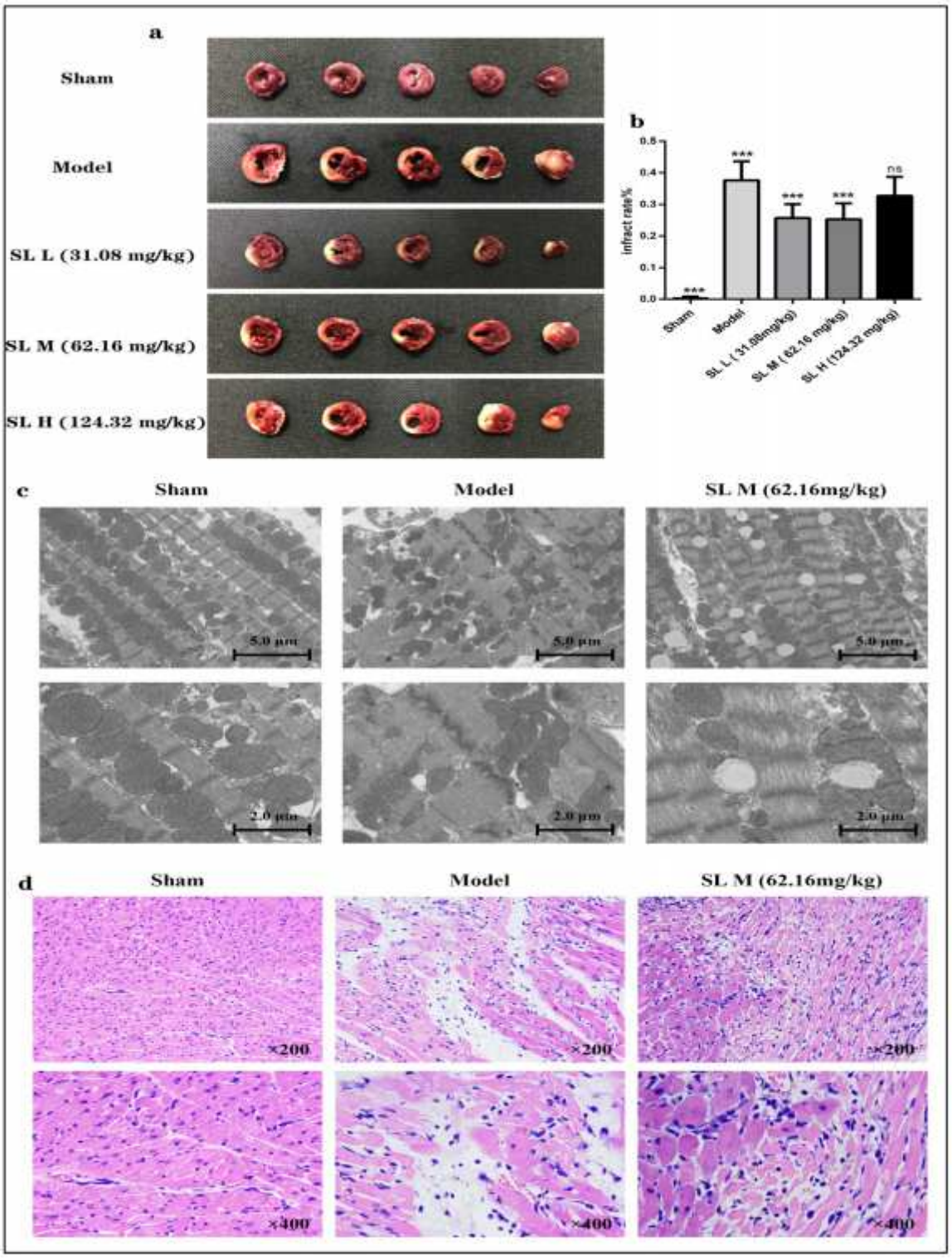

Figure 1

Efficacy evaluation of Shenlian extract (SL). (a, b) Effect of SL on infarct size in the experimental rats and the infarct rate as a percentage of the total size. Heart sections of the experimental rats stained with 2, 3, 5-triphenyltetrazolium chloride. Normal tissue was stained red, and infarcted tissue was pale. (c)

Ultrastructural changes of myocardial tissue and the effect of SL treatment (left, ×2000; right, ×50,000). (d)Myocardial histopathological changes and SL in rats (hematoxylin & eosin: left, ×200; right, ×400). *P < 0.05,**P < 0.01, ***P < 0.001.

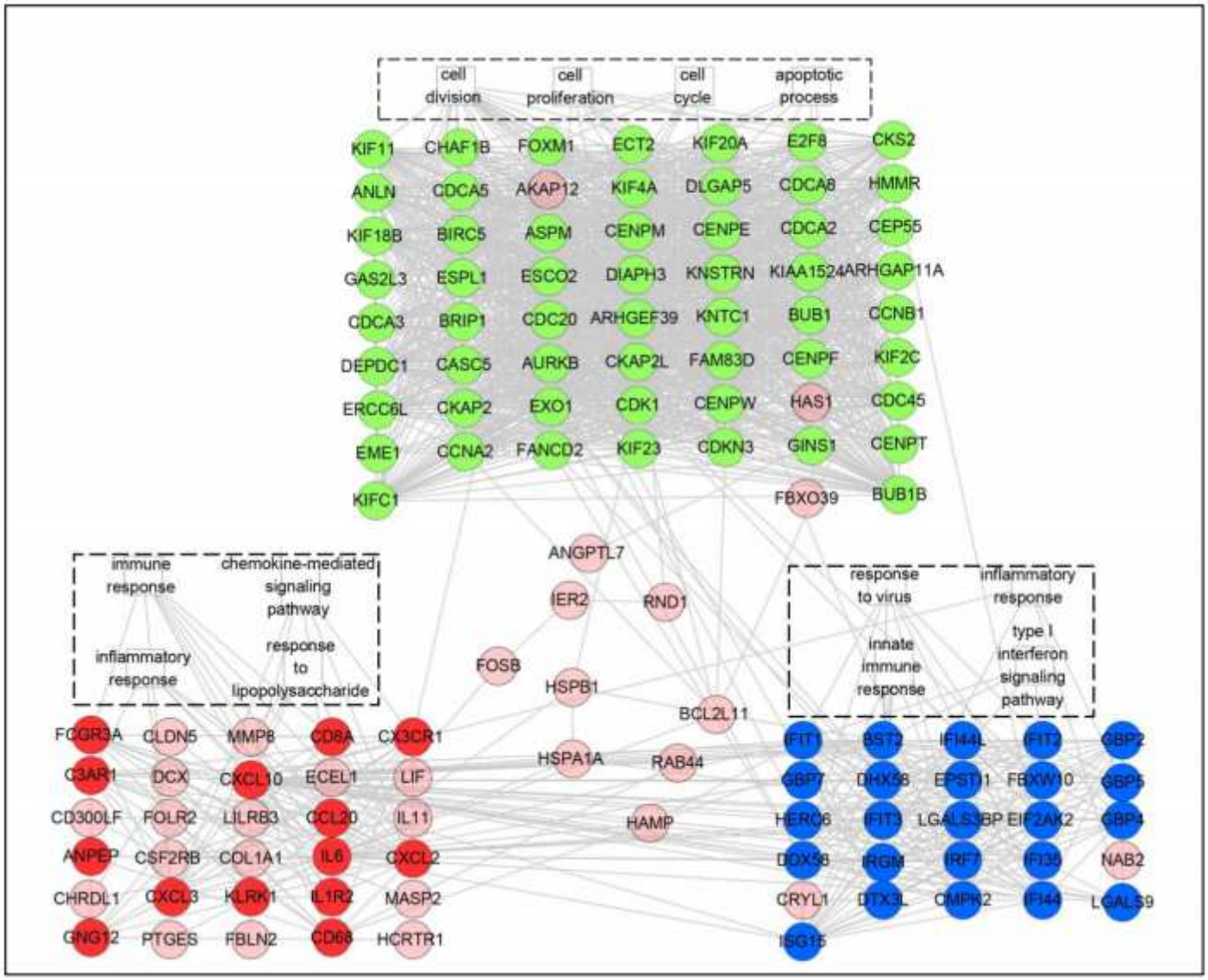

Figure 2

The enrichment analysis of genes altered by SL treatment following ultrafine particle-induced myocardial ischemic injury. The green, blue, and red nodes represent clusters 1, 2, and 3, respectively, and the pink nodes are the join points.

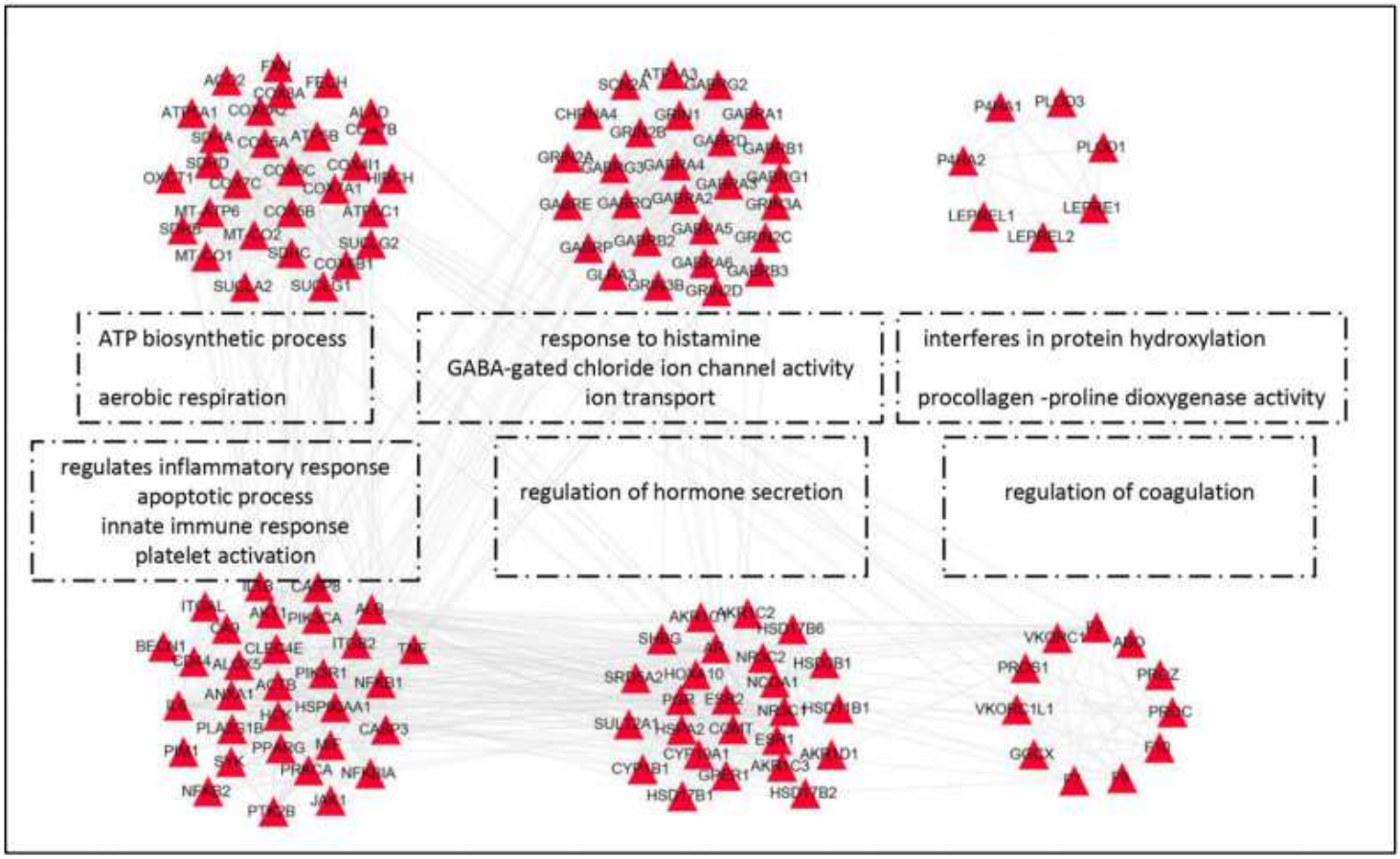

Figure 3

Enrichment analysis of Shenlian extract (SL). From top to bottom and from left to right, six clusters are respectively represented. The red triangles denote SL compound target, and the dashed boxes denote the biological function involving the corresponding cluster targets.

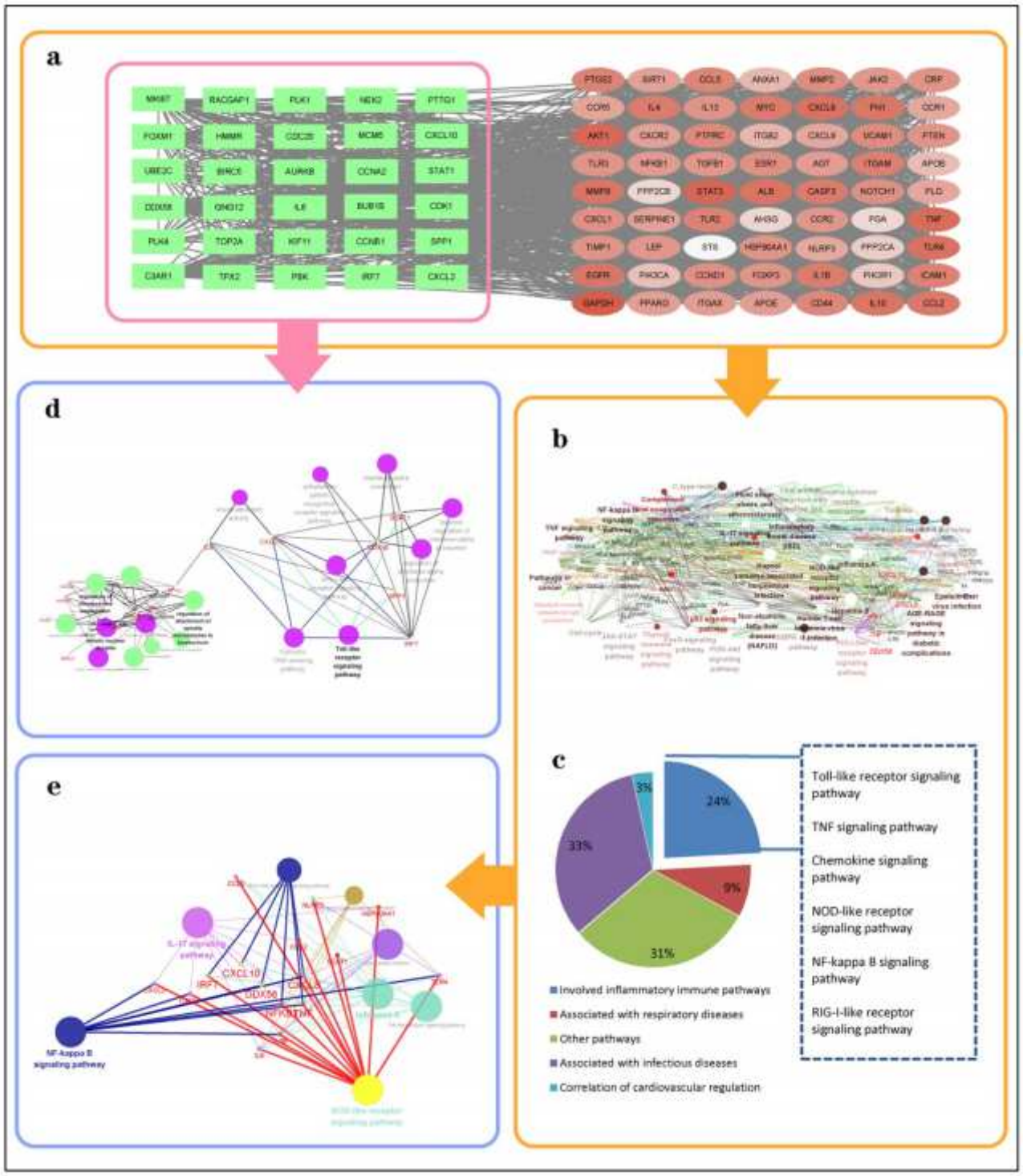

Figure 4

Enrichment analysis and target–pathway network construction for Shenlian extract for treating ultrafine particle-induced myocardial ischemic injury (a) Ninety-three core targets, including 30 green genes identified by our transcriptome research. (b, c) Pathway enrichment analysis of the 93 core targets. (d) The enrichment analysis of 30 transcriptome genes among core targets. (e) Key pathways of core target enrichment.

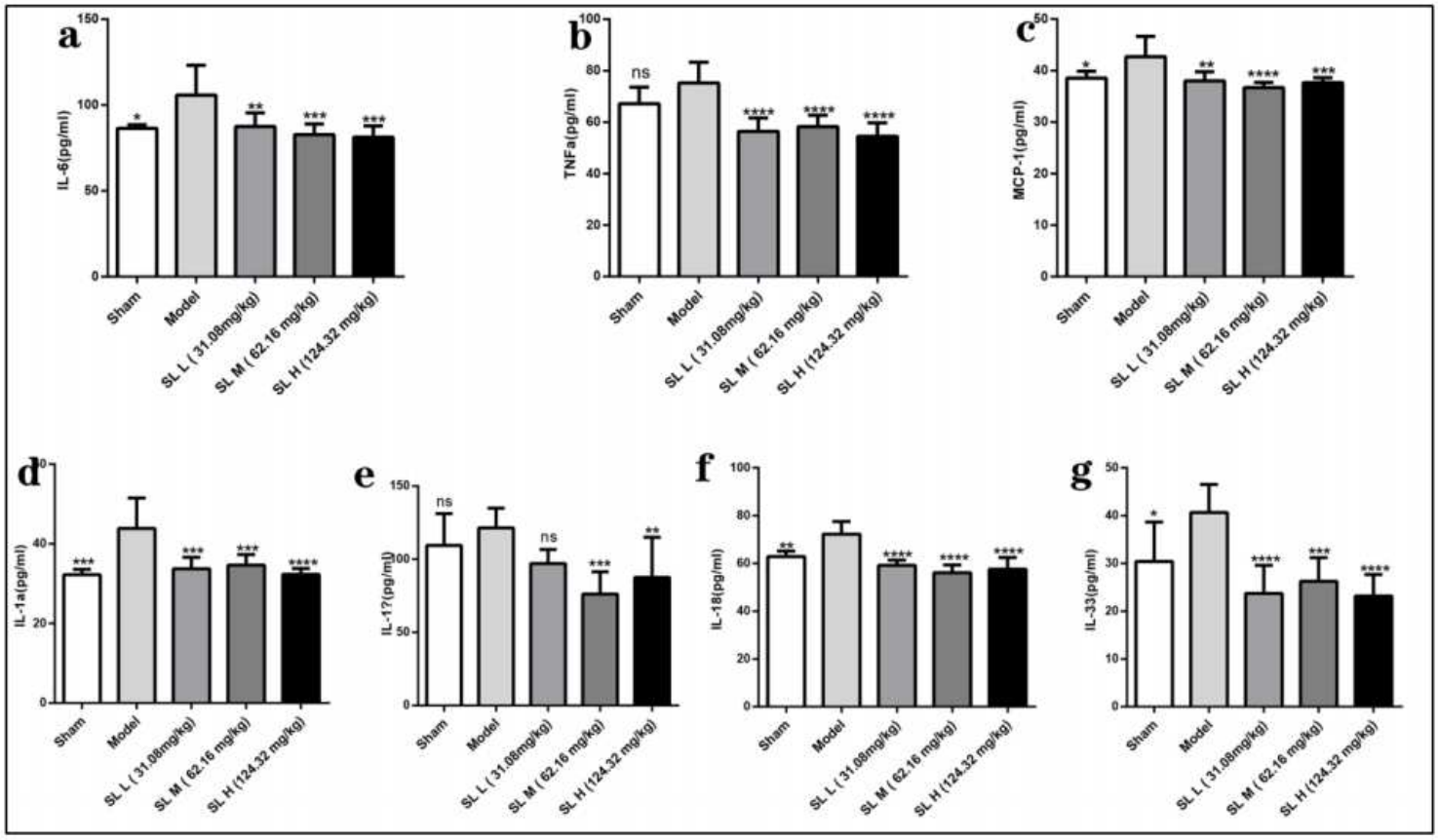

Figure 5

Expression of inflammatory factors and NLRP3 inflammasome-associated downstream cytokines. (a-c) The changes of inflammatory cytokine interleukin (IL)-6, tumor necrosis factor (TNF)-α, monocyte chemoattractant protein-1 (MCP)-1 levels in the serum of rats and the effects of Shenlian extract (SL). (d-g) Quantitative reverse results of interleukin (IL)-1α, IL-1β, IL-18, and IL-33 in the serum of rats. *P < 0.05, **P < 0.01, ***P < 0.001,****P < 0.0001.

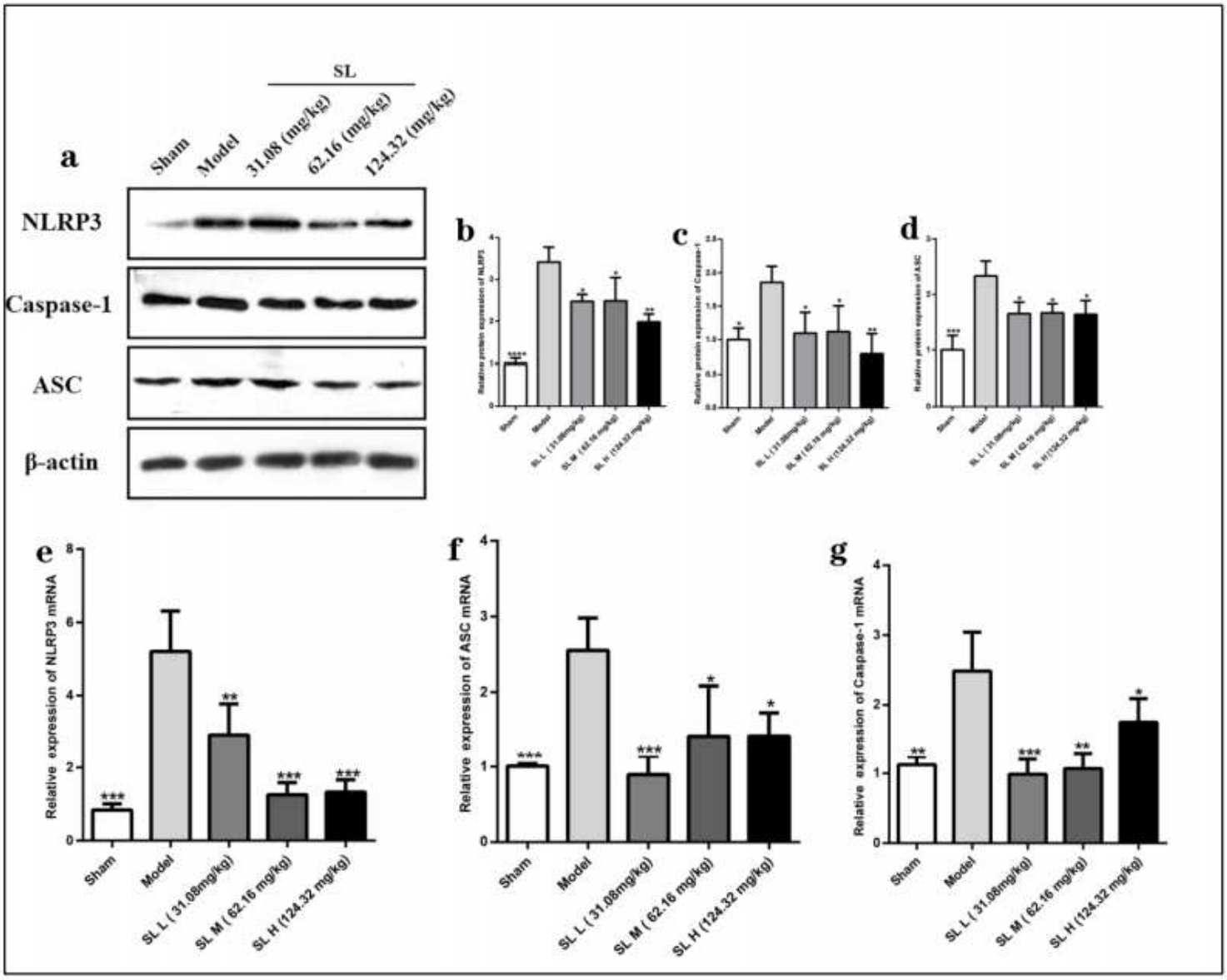

Figure 6

The expression of NLRP3 inflammasome. (a- d) Expression of NLRP3 inflammasome-associated proteins in the myocardial tissue of rats (n = 3, x ± s). (e-g) Expression of NLRP3 inflammasome-associated mRNA in the myocardial tissue of rats (n = 3, x ± s). *P < 0.05, **P < 0.01, ***P < 0.001.